JOURNAL OF GUIDANCE, CONTROL, AND DYNAMICS
Vol. 15, No. 6, November-December 1992

Experimental Demonstration of a Classical Approach to Flexible Structure Control

Bong Wie*
Arizona State University, Tempe, Arizona 85287

This paper describes the results of active structural control experiments performed for the ACES testbed at NASA Marshall Space Flight Center as part of the NASA Control-Structure Interaction Phase I Guest Investigator Program. The experimental results successfully demonstrate the effectiveness of a "dipole" concept for line-of-sight control of a pointing system mounted on a flexible structure. The simplicity and effectiveness of a classical "single-loop-at-a-time" approach for the active structural control design for a complex structure such as the ACES testbed are demonstrated. Consequently, the theoretical aspects of large space structure control problems are not elaborated in this paper.

I. Introduction

THIS paper describes ground experiments conducted for the Advanced Control Evaluation for Structures (ACES) testbed at the NASA Marshall Space Flight Center, under the NASA Control-Structure Interaction (CSI) Phase I Guest Investigator Program.[1] State-space methods for control design of flexible space structures have been emphasized in the literature and more widely explored than a classical method, as evidenced by all of the prior control experiments conducted for the ACES.[2-9] However, this paper describes the results of testing a classical controller[10] for the ACES testbed. During tests, particular emphasis was placed on 1) understanding the fundamental nature of control-structure interaction problems, and 2) exploring the effects of many simplifying assumptions on a realistic complex structure such as the ACES. Consequently, the theoretical aspects of large space structure control problems are not elaborated in this paper.

The overall objective of the control-structure interaction research program is to develop and validate the technology needed to design, verify, and operate advanced space vehicles with significant structural flexibility.[1] Some unique features of the technical approach employed to meet such overall objectives and to accomplish a successful experiment are summarized as follows:

1) A classical single-loop-at-a-time control design approach[11-14] was employed for the ACES with multiple actuators and sensors, while modern state-space multivariable control design approaches were employed in Refs. 2-9.

2) Analytical models were used for the classical control design, while experimentally identified, state-space models were used for the state-space control designs in Refs. 6-9.

3) The primary goal of verifying the simplicity of the classical control design approach for flexible structure control in achieving moderate performance and stability, with minimum controller complexity and minimum design efforts, has been accomplished, as evidenced by the experimental results compared with the test results presented in Refs. 2-9.

4) In particular, the simplicity and effectiveness of a dipole concept for disturbance accommodating control of flexible structures[13,14] has been successfully demonstrated for the ACES testbed which had been hampered by an uncontrolled but disturbed 0.15-Hz dominant mode.[2-5]

Received June 17, 1991; presented as Paper 91-2696 at the AIAA Guidance, Navigation, and Control Conference, New Orleans, LA, Aug. 12-14, 1991; revision received Dec. 31, 1991; accepted for publication Jan. 2, 1992.

*Professor, Dept. of Mechanical and Aerospace Engineering. Associate Fellow AIAA.

The remainder of this paper is organized as follows. Section II describes the ACES test facility. Section III discusses classical control design for the ACES, and Sec. IV presents the experimental results. Section V further discusses some fundamental issues in control design for large space structures. In Sec. VI, the dipole concept, successfully demonstrated for the ACES, is proposed for the Hubble Space Telescope with a pointing control problem caused by persistent solar-array excitation at 0.12 Hz and 0.66 Hz,[15] which is very similar to the ACES's 0.15-Hz problem. In the Appendix, the classical control design approach employed for the experiment is summarized.

II. ACES Testbed

In this section, the ACES testbed and its objectives are briefly described. A detailed description of the ACES facility and previous experimental results by other control researchers can be found in Refs. 2-9.

ACES System Description

The basic configuration of the ACES test facility is shown in Fig. 1. The basic component is a 2.27-kg, 13-m deployable astromast which served as the flight backup magnetometer boom for the Voyager spacecraft. It is a symmetric beam

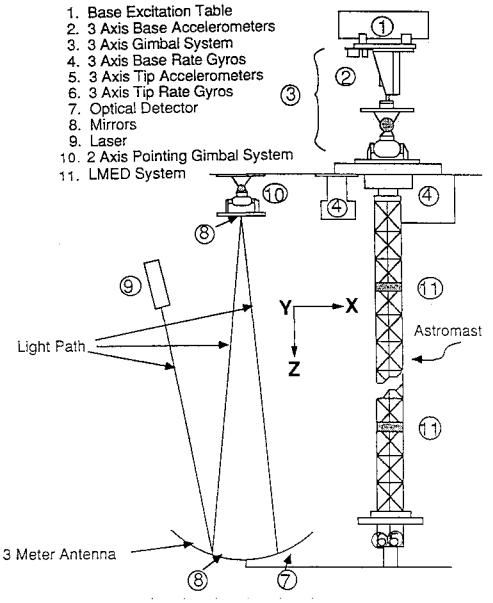

Fig. 1 ACES ground test facility.

Table 1 ACES structural mode descriptions

Mode, Hz	Description
0.14	1st astromast X bending
0.15	1st astromast Y bending
0.63	2nd astromast Y bending
0.75	2nd astromast X bending
0.82	3rd astromast Y bending
1.04	3rd astromast X bending
1.41	Antenna torsion
1.51	IMC gimbals
2.35	Antenna torsion + astromast bending
2.49	Antenna torsion + astromast bending
2.73	Astromast bending

which is triangular in cross section. The astromast has the equivalent continuous beam parameter of $EI = 2.31e8$ Nm^2. Appendages are attached to the astromast to emulate the closely spaced modal frequencies characteristic of large space structures. The appendages consist of an antenna and two counterbalance legs. The overall system has 43 structural modes under 8 Hz. Table 1 lists some of the dominant modes of the ACES structure.

The base excitation table (BET) is hydraulically driven to provide two-axis translational disturbances at the point where the astromast is attached to the overhead structure of the building. Several disturbances, representative of an actual space environment, can be provided by the BET. Later in this paper, two of these disturbances utilized in the experiment will be referred to as 1) BET pulse (thruster firings) and 2) BET step (crew motion disturbance).

The advanced gimbal system (AGS) is a precision, two-axis gimbal system designed for high-accuracy pointing applications, augmented by a third gimbal with a torquer and air-bearing system for azimuth control. The AGS provides torque actuation at the base mounting plate of the astromast in response to voltage command over the range of ± 10 V. The AGS torquers operate over ± 30 deg, saturate at 50 Nm of torque, and have bandwidths in excess of 50 Hz. Rate gyros are provided at the base and tip of the astromast, and they measure three-axis angular rates at each location. The AGS and the rate gyros at the base become collocated actuator/sensor pairs.

The linear momentum exchange devices (LMED) are proof-mass actuators which produce translational forces in two axes at each location, as shown in Fig. 1. Each LMED has a collocated accelerometer and a proof-mass position transducer. The moving mass of 0.75 kg contains permanent magnets which can move ± 3 cm over a voice coil actuator driven by a constant current source amplifier. Each LMED can deliver a peak force of 90 N; however, over the ± 10 V range of the control input, a maximum continuous force of 18 N is available. The force applied to the proof mass appears as a reaction force to the structure.

An optical system is provided to measure two-axis angular displacement of the antenna frame and thus monitor the line-of-sight pointing performance. The system consists of a laser source, two mirrors, and a two-axis optical detector. One of the mirrors is mounted on a two-axis pointing gimbal so the system can be used as a closed-loop image motion compensation (IMC) controller in addition to an optical performance sensor. The objective of this setup is to test an IMC controller which will minimize the laser-beam pointing error; this setup is representative of a secondary-mirror pointing control system of a large telescope.

A digital computer with a sampling rate of 50 Hz is provided to implement digital controllers and to store and post-process test results.

ACES Testbed Objectives

Similar to control experiments reported in Refs. 2–9, the primary goals of control design to be verified for the ACES testbed were 1) to reduce the IMC line-of-sight error (i.e., to point the laser beam in the center of the detector) in the presence of two representative disturbances, 2) to ensure that the controller has a practical size, and 3) to ensure that the controller is tolerant of model uncertainties.

The performance measures employed to evaluate the controller effectiveness include the detector response, the base rate gyro response, and the controller complexity. The primary performance criterion was the IMC line-of-sight pointing accuracy.

During the previous experiments conducted by other researchers for the ACES,[2-5] several problems were encountered. One of such problems was described in Ref. 4 as "An unmodeled mode appeared as the dominant mode at the detector. Since the detector error was intended to be the evaluation parameter, the appearance of the unmodeled mode was disastrous to the original evaluation plan. The mode (0.15 Hz) did not destabilize any of the controllers; on the other hand, no controller attenuated the mode."

This 0.15-Hz mode problem, however, was not encountered by other CSI Guest Investigators (e.g., see Refs. 6–9) since their controllers were not tested for the so-called BET step disturbance which is one of three representative disturbances available for the ACES.

One of the major contributions of this paper is to show that such a control problem encountered during the previous experiments was actually caused by the "nearly uncontrollable" but "significantly disturbable" 0.15-Hz mode. The mode is nearly uncontrollable by the AGS torque input and completely uncontrollable by the IMC gimbals. However, it can be excited or disturbed significantly by the BET step disturbance and can be observed by the IMC detector.

This paper will show that a simple IMC controller utilizing the dipole concept[13,14] can easily rectify such an uncontrollable but disturbable mode problem. This paper will also show that the pointing control problem recently encountered by the Hubble Space Telescope[15] is very similar to the ACES control problem with the uncontrolled but disturbed mode. Consequently, a simple controller utilizing the dipole concept is proposed for the Hubble Space Telescope.

III. Classical Control Design

The first step in control system design is to obtain a mathematical model of the physical system to be controlled. In

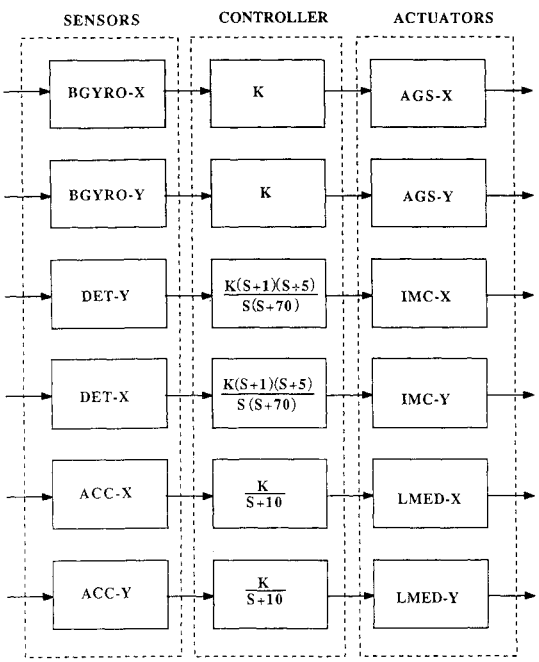

Fig. 2 Classical SISO controller for the ACES.

general, a finite element model of a flexible structure is represented by

$$M\ddot{q} + Kq = f \tag{1}$$

where M is a positive definite mass matrix, K a positive semi-definite stiffness matrix, q a generalized nodal coordinate vector, and f a vector of external forces and/or torques.

Equation (1) is transformed into the modal equation:

$$\ddot{\eta} + \Omega^2\eta = \Phi^T f \tag{2}$$

where η is a modal coordinate vector, $\Omega = \text{diag}(\omega_i)$, and ω_i the ith modal frequency, and Φ the modal matrix.

The mathematical model of the ACES provided by the NASA Marshall Space Flight Center includes the modal frequencies and mode shapes of the lowest 43 modes, and transfer function models of the ACES were used for classical control design.

Figure 2 illustrates a classical control system architecture selected for the ACES. Basically, the control system consists of six actuators and six sensors without cross feedback. The control inputs are the X- and Y-axis torques of the AGS gimbals, the X- and Y-axis forces of LMED located at the lower section of the astromast, and X- and Y-axis torques of the IMC gimbals. The sensor measurements consist of the X- and Y-axis base rate gyros (BGYRO), the X- and Y-axis accelerometer (ACC) outputs of the LMED, and the X- and Y-axis detector (DET) position outputs.

The classical single-loop-at-a-time control design for the ACES is briefly described as follows:

1) The AGS-X to BGYRO-X (also the AGS-Y to BGYRO-Y) loop basically consists of a collocated torque actuator and angular rate sensor pair. Although the effect of phase lag at high frequencies, caused by actuator/sensor dynamics and control loop time delay, must be considered in practical control design, a collocated direct rate feedback controller, as shown in Fig. 2, was chosen for testing. Because of relatively weak cross-axis coupling, it is not necessary to cross feedback the BGYRO outputs to the AGS gimbals.

2) The IMC-X to DET-Y (also the IMC-Y to DET-X) transfer function plot[2] includes a few flexible modes near 1.5 Hz.

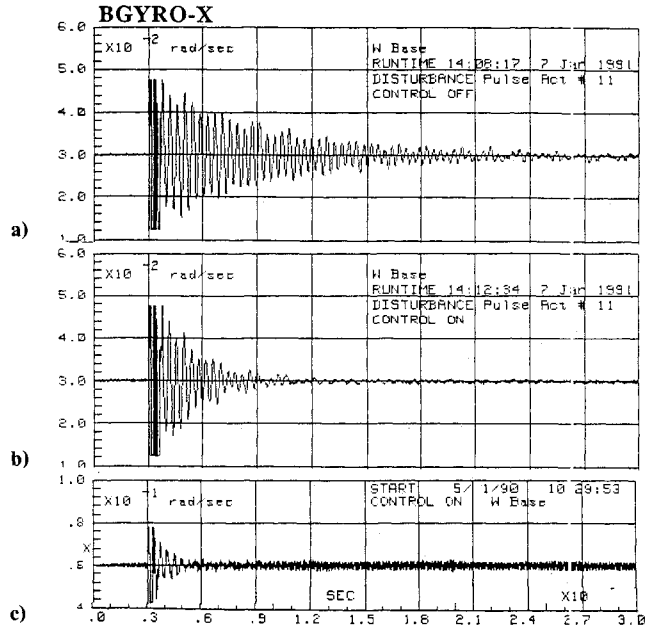

Fig. 3 BGYRO-X responses to BET-Y pulse: a) open loop; b) AGS closed loop with nominal gain; and c) AGS closed loop with high gain.

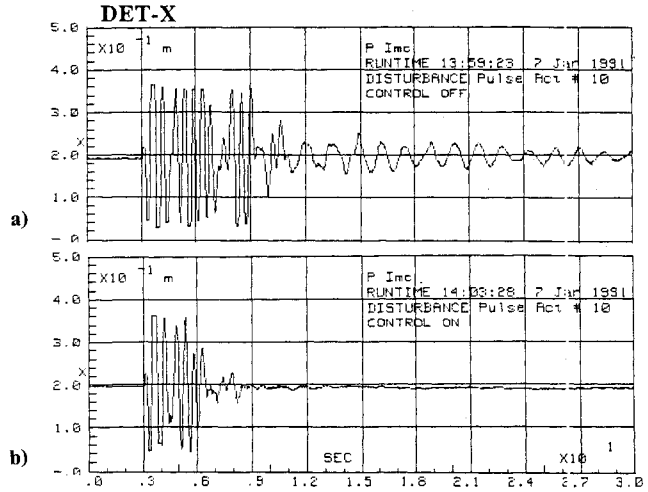

Fig. 4 DET-X responses to BET-X pulse: a) open loop and b) AGS closed loop with nominal gain.

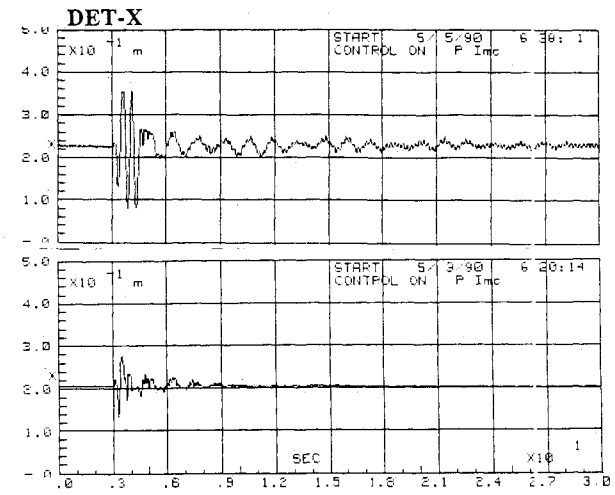

Fig. 5 DET-X responses to BET-X pulse: a) LMED closed loop and b) AGS + IMC closed loop with nominal gain.

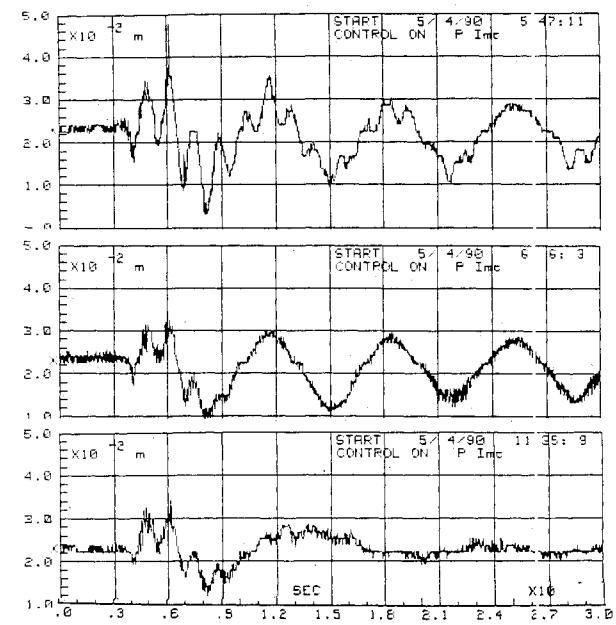

Fig. 6 DET-X responses to BET-X step: a) open loop; b) AGS + IMC (Fig. 2); and c) AGS + IMC (Fig. 7 with periodic-disturbance rejection dipole).

As a result, a classical PID controller, as shown in Fig. 2, was chosen for each IMC loop. Similar to the AGS loops, it is not necessary to cross feedback the detector (DET) outputs to the IMC gimbals.

3) As can be seen in Fig. 2, a direct acceleration feedback with first-order roll-off filtering was chosen for each collocated LMED and acceleration (ACC) control loop.[11]

In the Appendix, a classical single-input single-output (SISO) control design approach is summarized, with special emphasis on the concept of periodic disturbance rejection using a dipole, which will be shown to be very effective for accommodating the 0.15-Hz mode disturbance.

IV. Experimental Results

In this section, some of the experimental results are presented, which support the effectiveness of a simple classical controller, shown in Fig. 2, for achieving an excellent closed-loop performance.

Figure 3 shows a direct comparison of the open-loop and AGS closed-loop responses of BGYRO-X to a BET-Y pulse disturbance. Figure 3a shows the BGYRO-X open-loop response dominated by a 2.3-Hz mode. It can be seen in Fig. 3b that the 2.3-Hz mode is actively damped by the AGS controller (with nominal gain). However, an undesirable phenomenon of high-frequency instability is evident in Fig. 3c when the AGS rate gain is increased by a factor of two for more active damping of the 2.3-Hz mode. This experimental result confirms that there is no such a case as a perfect "collocated" rate feedback control with an infinity gain margin. Consequently, the AGS controller with nominal gain has a 6-dB gain margin.

Figure 4 shows a direct comparison of the open-loop and AGS closed-loop responses of DET-X to a BET-X pulse disturbance. Figure 4a shows the open-loop response of the detector output, dominated by two structural modes at 0.75 Hz and 2.3 Hz. As can be seen in Fig. 4b, significant performance improvement is achieved by the AGS controller (with nominal gain). Both the 0.75-Hz and 2.3-Hz modes are effectively damped out by the collocated rate feedback controller in the detector response.

Figure 5 shows the closed-loop responses of DET-X to a BET-X pulse disturbance. Figure 5a demonstrates the effectiveness of controlling the 2.3-Hz mode (but not the 0.75-Hz mode) by the LMED. As can be seen in Fig. 5b, very significant performance improvement in both the line-of-sight error and vibration suppression is achieved by the integrated AGS and IMC controller, as compared to the open-loop response shown in Fig. 4a.

Remark: The complete controller (i.e., AGS + IMC + LMED) has also been tested, resulting in similar responses to those of the integrated AGS + IMC controller. Since the AGS controller does provide sufficient active damping to structural modes, it is unnecessary, from the practical viewpoint, to use both the LMED and AGS controllers simultaneously. Thus, the experimental results of the complete controller are not emphasized in this paper.

Based upon the experimental results summarized in Figs. 3–5, it may be fair to say that an excellent closed-loop performance has been achieved by a rather simple classical controller shown in Fig. 2, compared to other experimental results reported in Refs. 2–9.

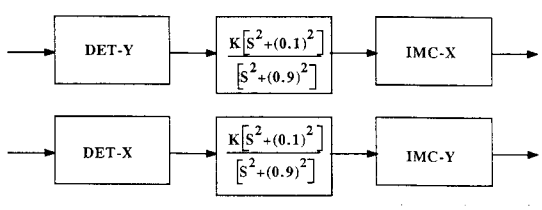

Fig. 7 IMC controller with periodic-disturbance rejection dipole.

Table 2 HST modal data (pitch/yaw axes)

Mode number	ω_i, Hz	Modal gain, K_i Pitch	Yaw
1	0.120	0.018	0.025
2	0.432	0.012	0.000
3	0.660	0.000	0.079
4	0.912	0.057	0.000
5	1.079	0.000	0.029
6	2.508	0.000	0.013
7	10.834	0.024	0.104
8	12.133	0.155	−0.320
9	13.201	−1.341	−0.110
10	14.068	−1.387	−0.217
11	14.285	−0.806	−1.516
12	15.264	−0.134	0.170

However, a case of further interest is the case with the BET step disturbance. Figure 6 compares the open-loop and closed-loop responses of DET-X to a BET-X step disturbance. Figure 6a shows the open-loop response, dominated by a 0.15-Hz mode and other lower-frequency modes. Figure 6b shows the baseline integrated IMC + AGS closed-loop response, which is undoubtedly unacceptable. The reason for such unacceptable (also unpredicted) closed-loop performance is due to the presence of the 0.15-Hz mode which can be seen in both Figs. 6a and 6b.

Several prior ACES experiments had been hampered by the uncontrolled 0.15-Hz mode.[2–5] It is important to note that such a low-frequency mode is nearly uncontrollable by the AGS torque input, nearly unobservable by the base rate gyros, and completely uncontrollable by the IMC gimbals. However, it can be excited or disturbed significantly by a BET step disturbance and can be observed by the IMC detector which is not collocated with the AGS and the rate gyros at the base.

For the purpose of IMC controller redesign, the 0.15-Hz mode excitation can be simply considered as a persistent external disturbance. To isolate such an undesirable disturbance, a new IMC controller shown in Fig. 7 was designed. The new controller simply includes a dipole for disturbance rejection with the pole at $s = \pm j\,0.9$. The zero corresponding to the dipole is placed at $s = \pm j\,0.1$. A detailed discussion of this dipole concept can be found in the Appendix.

The closed-loop test result shown in Fig. 6c clearly demonstrates the effectiveness of the redesigned IMC controller for rejecting the 0.15-Hz mode in the detector output.

V. Discussion

State-space methods for control design of flexible space structures have been emphasized by many control researchers and more widely explored than classical methods (e.g., see Refs. 2–9). This arises from the convenience of obtaining a compensator for the whole system given one set of weighting parameters. However, the fundamental question remains how to choose these parameters and what choice provides the "best" optimal design. The designer must find an acceptable set of parameters for a "good" optimal design. The use of state-space methods for control design usually results in a compensator of the same order as the system to be controlled. This means that for systems having several flexible modes, the compensator adds compensation even to modes that are stable and need no compensation. This may result in a high-order compensator design.

In classical design, on the other hand, a compensator must be constructed piece by piece, or mode by mode. As demonstrated in the preceding sections, the classical design is particularly convenient for the control of flexible space structures with properly selected collocated actuator/sensor pairs. The concept of nonminimum-phase compensation also provides an extremely convenient way of stabilizing unstably interacting flexible modes for the case in which actuators and sensors are not collocated, as discovered in Ref. 12 and also as demon-

strated experimentally in Ref. 14. The resulting compensator is usually of less order than the system to be controlled since not all flexible modes in a structure tend to be destabilized by a reduced-order controller.

A helpful characteristic of most flexible space structures is their inherent passive damping. This gives the designer the opportunity of phase stabilizing significant modes and to gain stabilize all other higher-frequency modes which have less influence on the structure, as demonstrated in the preceding sections (e.g., see Fig. 3).

VI. HST Pointing Control Problem

In this section, the solar-array thermal flutter problem of the Hubble Space Telescope (HST) is briefly discussed to emphasize the significance of the experimental results for the ACES in accommodating the 0.15-Hz disturbance. Detailed discussions of the HST pointing control system and its solar-array excitation problem can be found in Refs. 15–18.

According to Ref. 15, there appear to be two types of thermal flutter of the 20-ft-long solar arrays: 1) an end-to-end bending oscillation at 0.12 Hz when the spacecraft passes between sunlight and shadow, and 2) a sideways bending oscillation at 0.66 Hz that occurs on the day side of the Earth. The effect of such solar-array vibration is that the pointing performance of the spacecraft is significantly degraded, especially, in the pitch and yaw axes.

The HST can be represented in transfer-function form for each control axis as follows:

$$\frac{\theta(s)}{u(s)} = \frac{1}{Is^2} + \sum_{i=1} \frac{K_i/I}{s^2 + 2\zeta\omega_i s + \omega_i^2} \tag{3}$$

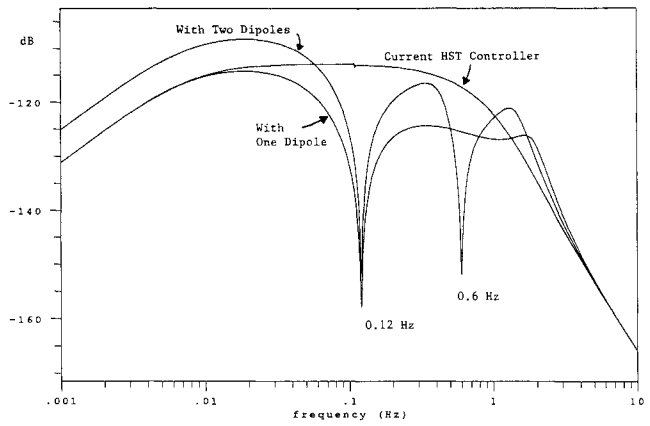

Fig. 8 Closed-loop Bode magnitude plots for the Hubble Space Telescope.

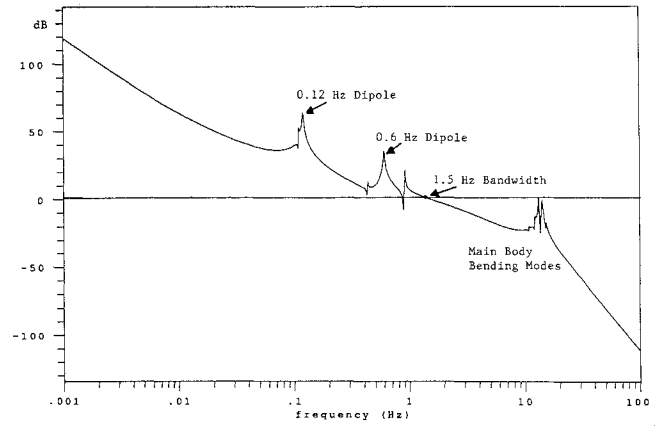

Fig. 9 Loop transfer-function magnitude plot for a proposed controller with two dipoles for disturbance rejection at 0.12 Hz and 0.66 Hz.

where θ is the attitude error output, u the reaction wheel control torque input, s the Laplace transform variable, I the spacecraft inertia, K_i the ith flexible mode gain, ω_i the ith flexible mode frequency in rad/second, and ζ is the passive damping ratio assumed as 0.005. Table 2 lists the pitch/yaw axes modal data of the HST.

The baseline PID controller for each axis, not including a roll-off filter in the rate loop,[15-17] can be expressed as

$$u(s) = -I(K_P + K_I/s + K_D s)\theta(s)$$

where $K_P = 9$, $K_I = 0.45$, and $K_D = 4.5$ for both pitch and yaw axes. The controller is digitally implemented with a 25-ms sampling period and the control loop has a 7-ms pure time delay.

The following new controller with two dipoles is proposed for the HST to accommodate both the 0.12-Hz and 0.66-Hz disturbances:

$$u(s) = -I(K_P + K_I/s + K_D s) \times 0.5 \frac{[(s/z_1)^2 + 2\zeta_{z_1} s/z_1 + 1][(s/z_2)^2 + 2\zeta_{z_2} s/z_2 + 1]}{[(s/p_1)^2 + 2\zeta_{p_1} s/p_1 + 1][(s/p_2)^2 + 2\zeta_{p_2} s/p_2 + 1]}\theta(s)$$

where

$$z_1 = 2\pi(0.08), \qquad \zeta_{z_1} = 1.00$$

$$p_1 = 2\pi(0.12), \qquad \zeta_{p_1} = 0.01$$

$$z_2 = 2\pi(0.50), \qquad \zeta_{z_2} = 0.20$$

$$p_2 = 2\pi(0.66), \qquad \zeta_{p_2} = 0.01$$

and the overall loop gain is not reduced by a factor of two if only one dipole is employed.

Figure 8 shows a direct comparison of the closed-loop frequency responses from the yaw-axis disturbance to the pitch-attitude output for three different cases: 1) the baseline PID controller, 2) PID + one dipole at 0.12 Hz, and 3) PID + two dipoles. It can be seen that as compared to the baseline PID controller, the new controller with one dipole has a 40 dB more gain attenuation at 0.12 Hz and an additional 10-dB attenuation at 0.66 Hz without significantly affecting the low- and high-frequency gains. The new proposed controller with two dipoles has additional 40-dB gain attenuation at both 0.12 Hz and 0.66 Hz, as compared to the baseline PID controller. As can be seen in Fig. 9, the proposed controller with two dipoles has the same 1.5-Hz bandwidth as the baseline PID controller. The high-frequency structural modes near 14 Hz are in fact phase stabilized by the phase-lag effects of the sampling and time delay.

VII. Conclusions

The experimental results for the ACES structure located at the NASA Marshall Space Flight Center have been presented. The primary objective of verifying the simplicity and effectiveness of the classical single-loop-at-a-time approach for controlling a complex flexible structure such as the ACES has been accomplished. The simplicity and practicality of the "dipole" concept for persistent disturbance rejection control of flexible structures was successfully demonstrated.

Appendix: Classical SISO Design Approach

In this Appendix, a classical SISO control design approach, with special emphasis on a generalized structural filtering concept[12] and a dipole concept,[13] is summarized.

Successive Mode Stabilization

The design of a SISO feedback control system for a flexible structure is carried out starting with the stabilization of a

rigid-body mode and/or dominant flexible modes and subsequent analysis and stabilization of unstably interacting flexible modes. Feedback control with a noncollocated actuator and sensor pair or with significant time delay generally results in the presence of unstably interacting flexible modes. After the unstably interacting modes have been identified, proper filtering to phase or gain stabilize those modes is then introduced. Also, active disturbance rejection filtering is synthesized to compensate for any persistent disturbances acting on the structure. Aided by the root locus method and/or Bode plots, and a certain amount of trial and error, a robust compensator design is obtained.

The classical SISO design based on successive mode stabilization can be divided into four steps:

1) Stabilization of a rigid-body mode and/or dominant flexible modes according to given time- or frequency-domain specifications (settling time, maximum overshoot, bandwidth, phase and gain margins).

2) Gain/phase stabilization of any unstably interacting or destabilized flexible modes.

3) Synthesis of active disturbance rejection filter and/or command preshaping filter.

4) Final tuning of the overall compensator.

The last step becomes necessary because the phase and gain characteristics of active disturbance rejection filtering as well as the stabilized modes in question exert their influence on all neighboring frequencies, which may include other modes. This presents a challenge as the number of modes to be stabilized becomes larger.

Phase and/or gain stabilization of an unstably interacting flexible mode can be achieved with the introduction of a roll-off filter and/or a generalized second-order filter of the following form in the feedback loop:

$$\frac{(s/z)^2 + 2\zeta_z s/z + 1}{(s/p)^2 + 2\zeta_p s/p + 1}$$

where s is the Laplace transform variable. Nonminimum-phase second-order shaping filters with negative ζ_z are of special interest for a certain class of noncollocated control problems, as discovered in Ref. 12.

Active Disturbance Rejection

After successful stabilization of the rigid-body mode and/or dominant flexible modes (as well as any other unstably interacting flexible modes), active disturbance rejection is then simply achieved by introducing into the feedback loop a disturbance model of the form

$$w(t) = \sum_i A_i \sin(p_i t + \phi_i)$$

with unknown magnitudes A_i and phases ϕ_i but known frequencies p_i. In general, the disturbance $w(t)$ can be described by a Laplace transformation $w(s) = N_w(s)/D_w(s)$, where $N_w(s)$ is arbitrary as long as $w(s)$ remains proper. The roots of $D_w(s)$ correspond to the frequencies at which the persistent excitation takes place. The inclusion of the disturbance model $1/D_w$ inside the control loop is often referred to as the internal modeling of the disturbance.

The presence of $1/D_w$ in the control loop results in the effective cancellation of the poles of $w(s)$, provided that no root of $D_w(s)$ is a zero of the plant transfer function. This is shown in the following closed-loop transfer function:

$$y(s) = \frac{1/D(s)}{1 + N_c(s)N(s)/D_c(s)D_w(s)D(s)}\, w(s)$$

$$= \frac{D_c(s)D_w(s)}{D_w(s)D_c(s)D(s) + N_c(s)N(s)} \frac{N_w(s)}{D_w(s)}$$

where we can see the cancellation of $D_w(s)$. Note that the numerator dynamics of the disturbance channel, which is not necessarily the same as $N(s)$, has been included in $N_w(s)$.

The compensator can be viewed as a series of individual first-order or second-order filters as follows:

$$\frac{N_c(s)}{D_c(s)} = \prod_i \frac{N_{c_i}(s)}{D_{c_i}(s)}$$

Each filter is designed to perform a specific task, such as the stabilization of a particular mode. In the same manner, a disturbance rejection filter can be designed that has a proper transfer function and uses the internal disturbance model $1/D_w$. Thus a proper numerator is chosen in the compensator to go with the disturbance model. The numerator is chosen to be of the same order as D_w so that there is a zero for each pole of the disturbance model $1/D_w$.

Each pole-zero combination of the disturbance rejection filter

$$\prod_i \frac{(s/z_i)^2 + 2\zeta_{z_i} s/z_i + 1}{(s/p_i)^2 + 1}$$

can be called a dipole, where ζ_{z_i} is included for generality. The filter thus consists of as many dipoles as there are frequency components in the persistent disturbance. The separation between the zero and the pole is generally referred to as the strength of the dipole. The strength of the dipole affects the settling time of the closed-loop system; in general, the larger the separation between the pole and zero of the filter the shorter the settling time. This is caused by the position of the closed-loop eigenvalue corresponding to the filter dipole. As the strength of the dipole is increased, this eigenvalue is pushed farther to the left, speeding up the response time of the disturbance rejection. Therefore, as the strength of the dipole is changed to meet a chosen settling time the compensation must be readjusted. A compromise has to be reached often between the the settling time and the stability of the compensated system.

Acknowledgments

This research was supported by the NASA Langley Research Center under the Control Structure Interaction (CSI) Phase I Guest Investigator Program. The author would like to thank Henry Waites and John Sharkey at the NASA Marshall Space Flight Center for their efforts in developing such an excellent test facility and for their technical assistance during tests. The technical support of Michael Dendy of Control Dynamics Company during tests is also acknowledged. The author is also very grateful to Jerry Newsom (CSI Program Manager) and Rudeen Smith-Taylor (CSI GI Program Manager) for supporting the advancement of classical control theory as applied to the CSI technology.

References

[1]Newsom, J. R., Layman, W. E., Waites, H. B., and Hayduk, R. J., "The NASA Controls-Structures Interaction Technology Program," IAF-90-290, 41st Congress of the International Astronautical Federation, Germany, Oct. 6-12, 1990.

[2]Waites, H., et al., "Active Control Technique Evaluation for Spacecraft (ACES)," Final Technical Rept., F33615-86-C-3225, NASA/MSFC and Control Dynamics Co., March 25, 1988.

[3]Pearson, J., and Waites, H., "Advanced Control Evaluation for Structures (ACES) Programs," *Proceedings of the 1988 American Control Conference,* June 1988, pp. 1448-1455.

[4]Jones, V. L., and Waites, H., "ACES Program: Lesson Learned," *Proceedings of the 1988 American Control Conference,* June 1988, pp. 1453-1455.

[5]Irwin, R.D ., "Application of FAMESS to a Large Space Structure Ground Test Facility," *Proceedings of the 1988 American Control Conference,* June 1988, pp. 1456-1461.

[6]Collins, E. G., Phillips, D., and Hyland, D. C., "Design and Implementation of Robust Decentralized Control Laws for the ACES Structure," *Proceedings of the 1990 American Control Conference,* May 1990, pp. 1449-1454.

[7]Slater, G., Bosse, A., and Zhang, Q., "Practical Experience with Multivariable Positivity Controllers for the ACES," *Proceedings of the 1990 American Control Conference,* May 1990, pp. 1445–1448.

[8]Balas, G., and Doyle, J., "Caltech CSI GI Year End Review," NASA CSI Guest Investigator First Year Review Meeting, Jan. 23–24, 1990, NASA Langley Research Center, Hampton, VA, pp. 479–550.

[9]Liu, K., and Skelton, R., "Experimental Verification of an Integrated Modeling and Control Strategy for Flexible Structures," NASA CSI Guest Investigator Final Review Meeting, April 5, 1991, Huntsville, AL, pp. 121–178.

[10]Wie, B., "Experimental Verification of a Classical SISO Approach to Flexible Structure Control," NASA CSI Guest Investigator Final Review Meeting, April 5, 1991, Huntsville, AL, pp. 179–218.

[11]Wie, B., "Active Vibration Control Synthesis for the COFS Mast Flight System," *Journal of Guidance, Control, and Dynamics,* Vol. 11, No. 3, 1988, pp. 271–276.

[12]Wie, B., and Byun, K., "New Generalized Structural Filtering Concept for Active Vibration Control Synthesis," *Journal of Guidance, Control, and Dynamics,* Vol. 12, No. 2, 1989, pp. 147–154.

[13]Wie, B., and Gonzalez, M., "Control Synthesis for Flexible Space Structures Excited by Persistent Disturbances," *Journal of Guidance, Control, and Dynamics,* Vol. 15, No. 1, 1992, pp. 73–80.

[14]Wie, B., Horta, L., and Sulla, J., "Classical Control System Design and Experiment for the Mini-Mast Truss Structure," *Journal of Guidance, Control, and Dynamics,* Vol. 14, No. 4, 1991, pp. 778–784.

[15]"Hubble Space Telescope SAGA Readiness Review Report," NASA Goddard Space Flight Center, Oct. 2, 1990.

[16]Dougherty, H., Tompetrini, K., Levinthal, J., and Nurre, G., "Space Telescope Pointing Control System," *Journal of Guidance, Control, and Dynamics,* Vol. 5, No. 4, 1982, pp. 403–409.

[17]Beals, G. A., Crum, R. C., Dougherty, H. J., Hegel, D. K., Kelley, T. L., and Rodden, J. J., "Hubble Space Telescope Precision Pointing Control System," *Journal of Guidance, Control, and Dynamics,* Vol. 11, No. 2, 1988, pp. 119–123.

[18]Wie, B., Liu, Q., and Bauer, F., "Classical and Modern Control Redesign for the Hubble Space Telescope," AIAA Guidance, Navigation, and Control Conference (Hilton Head, SC), Aug. 10–12, 1992.